Published in final edited form as:
Biomaterials. 2013 September ; 34(28): 6862–6870. doi:10.1016/j.biomaterials.2013.05.053.

The effect of lipid monolayer in-plane rigidity on *in vivo* microbubble circulation persistence

Sumit Garg, **Alex A. Thomas**, and **Mark A. Borden***
Department of Mechanical Engineering, Materials Science and Engineering Program, University of Colorado, Boulder, CO 80309

Abstract

The goal of this study was to increase *in vivo* microbubble circulation persistence for applications in medical imaging and targeted drug delivery. Our approach was to investigate the effect of lipid monolayer in-plane rigidity to reduce the rate of microbubble dissolution, while holding constant the microbubble size, concentration and surface architecture. We first estimated the impact of acyl chain length of the main diacyl phosphatidyl-choline (PC) lipid and inter-lipid distance on the cohesive surface energy and, based on these results, we hypothesized that microbubble stability and *in vivo* ultrasound contrast persistence would increase monotonically with increasing acyl chain length. We therefore measured microbubble *in vitro* stability to dilution with and without ultrasound exposure, as well as *in vivo* ultrasound contrast persistence. All measurements showed a sharp rise in stability between DPPC (C16:0) and DSPC (C18:0), which correlates to the wrinkling transition, which signals the onset of significant surface shear and gas permeation resistance, observed in prior single-bubble dissolution studies. Further evidence for the effect of the wrinkling transition came from an *in vitro* and *in vivo* stability comparison of microbubbles coated with pure DPPC with those of lung surfactant extract. Microbubble stability against dilution without ultrasound and *in vivo* ultrasound contrast persistence showed a monotonic increase with acyl chain length from DSPC to DBPC (C22:0). However, we also observed that stability dropped precipitously for all measurements on further increasing lipid acyl chain length from DBPC to DLiPC (C24:0). This result suggests that hydrophobic mismatch between the main PC lipid and the lipopolymer emulsifier, DSPE-PEG5000, may drive a less stable surface microstructure. Overall, these results support our general hypothesis of the role of in-plane rigidity for increasing the lifetime of microbubble circulation.

Keywords

wrinkling transition; hydrophobic mismatch; monolayer cohesion energy; perfluorobutane; polyethylene glycol PEG

Introduction

Ultrasound (US) medical imaging is safe, inexpensive, portable, and offers excellent spatial resolution and real-time visualization, but its use for advanced diagnostic imaging is

*Corresponding author address: 1111 Engineering Drive Boulder, CO 80309-0427 Phone: 303.492.7750 Fax: 303.492.3498 .

hampered by poor soft tissue contrast, which makes the images difficult to interpret. Tissue contrast can be improved by intravascular injection of microbubble ultrasound contrast agents [1], but their short circulation lifetime somewhat limits their broad use in clinical cardiology and radiology. In this study, we overcome this limitation as we significantly prolonged the circulation lifetime of microbubbles by making changes in the microbubble lipid shell composition.

Lipid-coated microbubbles meet two of the key performance criteria for ultrasound contrast agents: biocompatibility and strong ultrasonic backscatter [2-4]. They are spherical gas cores stabilized by polymer-grafted lipid monolayer shells. Lipids monolayers naturally occur in the human body, e.g. the alveolar lining, where they stabilize the gas/liquid interface by reducing surface tension and yet provide a flexible membrane that can adjust to area changes during the breathing cycle. Due to the gas core and soft shell, lipid-coated microbubbles can volumetrically oscillate under low-intensity US and appear bright on the video screen of the ultrasound scanner [5-7]. They have high ultrasonic backscatter because the intra-lipid interactions are not strong enough to significantly dampen the radial oscillations during acoustic stimulation. Despite these advantages, the major limitation is that the microbubble circulation lifetime in the vasculature is relatively short. For example, a bolus injection of Definity® (Lantheus Medical Imaging, Billerica, MA) typically provides only 3-5 minutes of ultrasound contrast [8].

There are two major mechanisms for microbubble clearance in the vasculature: phagocytosis and dissolution. Phagocytosis occurs through the mononuclear phagocyte system (MPS), and is believed to be mediated by the alternative (innate) complement pathway through fixation of protein fragment C3b (Fig. 1). Evidence for the role of phagocytosis has been reported from positron emission tomography (PET) imaging studies of microbubble pharmacokinetics and biodistribution [9, 10], which have shown rapid uptake in the lungs, liver and spleen. To reduce complement activation and macrophage uptake, microbubbles are prepared with neutral surface charge [11], which reduces non-specific protein adsorption. In addition, polyethylene glycol (PEG) brushes are attached to the microbubble surface to provide steric hindrance against protein adsorption and complement fixation [2, 12, 13].

Despite these advances in engineering of the microbubble surface architecture and chemistry to reduce complement activation and phagocytosis, microbubble lifetime *in vivo* remains relatively short [14-17]. We therefore focus here on design modifications of the lipid shell to delay dissolution. Dissolution of microbubbles occurs as the gas core diffuses into the bloodstream and is eliminated from the body through the lungs [18]. The rate of dissolution has been significantly reduced by use of low-solubility perfluorocarbon gases [19-21]. In theory, the use of higher fluorocarbons can further impede dissolution, but in practice this approach is impossible because higher fluorocarbons are in the liquid state under physiological conditions. Therefore the limit of this approach has been reached, and an alternative strategy is needed. We hypothesize that modification of the microbubble shell can enhance the resistance to dissolution.

Our approach is focused on increasing the lateral cohesive forces between the phospholipid molecules to enhance microbubble shell gas permeation resistance and its stability against collapse [4, 22-24]. Lipid packing density is affected by lipid acyl chain saturation and length. Unsaturated lipid has a kink (*cis* isomer) in the acyl chain and does not pack as well as the straight (*trans* isomer) saturated lipid. Clinical formulations of microbubbles already use saturated lipids with neutral headgroups. However, prior *in vivo* work has not given enough attention to the lipid acyl chain length, which can significantly enhance the attractive forces between the lipid molecules.

Research has shown that increasing the acyl chain length can have significant effects on the physiochemical behavior of lipid monolayers, and can prolong the time for dissolution of an individual lipid-coated microbubble in a degassed medium [22]. Longer chain lipids have been shown to have increased bending modulus [25] and degree of acyl chain order [26], and reduced lateral density fluctuations [27] owing to the enhanced van der Waals attraction. In addition, longer acyl chains can increase the lipid membrane thickness [28] and provide a thicker barrier for solute permeation. For monolayers on microbubbles, it has been demonstrated that longer chain lipids increase the surface yield shear and shear viscosity [29, 30]. Microbubbles in these studies were seen to hold a free projection formed by micropipette aspiration, indicating a strong monolayer cohesion and in-plane rigidity that overcomes surface tension, which would tend to retract the projection. Interestingly, microbubbles coated with longer acyl chains show discontinuous dissolution, with wrinkling and spontaneous restoration of sphericity as the microbubble shrinks [4]. This observation of a “wrinkling transition”, a hallmark of in-plane rigidity, suggests that longer acyl chains on microbubbles enhance the resistance to gas permeation [31, 32] and monolayer collapse [4], thereby slowing the dissolution process for individual microbubbles [4, 16, 22, 31].

Although prior bench-top studies have shown greater microbubble stability for shells comprising longer chain lipids, the biomaterials paradigm has not yet been completed since the effect has not been demonstrated *in vivo*. We hypothesized that increasing the lipid acyl chain length would result in a direct increase in microbubble circulation persistence. Thus, our hypothesis directly links microbubble composition to biomedical performance. To test this hypothesis, we measured *in vitro* stability with and without ultrasound exposure for diluted microbubble ensembles encapsulated by phosphatidyl-choline (PC) lipids with acyl chains ranging from 16 to 24 carbons, as well as the *in vivo* ultrasound contrast persistence in healthy, immune-competent mice following intravenous injection. PEG-lipid content was fixed to isolate the effects of PC acyl chain length. Additionally, processing history (and hence microstructure) was assumed to be equal for the microbubbles, as all of the formulations were generated and size selected to 4-5 μm diameter by the same procedure. This allowed us to examine our hypothesis on the effect of acyl chain length on *in vivo* circulation persistence.

To further test the hypothesis of the role of in-plane rigidity, we compared the *in vitro* and *in vivo* stability of microbubbles coated with pure DPPC (no lipopolymer) and a natural lung surfactant extract, Survanta® (Abbott Nutrition). Lung surfactant is a complex mixture of lipids and proteins lining the alveoli [33]. Survanta comprises dipalmitoyl-phosphatidylcholine (DPPC) and other lipids, as well as the surfactant proteins SP-B and SP-C. Pure DPPC is able to reach near zero surface tension, but it collapses via a fracture mechanism that limits the compressive strength [34]. The addition of unsaturated lipids leads to two-phase coexistence with solid DPPC domains surrounded by a more fluid monolayer matrix [35], allowing for in-plane shearing and low compressive strength [36]. The surfactant proteins SP-B and SP-C modify the microstructure of the inter-domain region of the two-phase monolayer to provide in-plane rigidity, and this rigidity leads to higher compressive strength where the monolayer collapses via a buckling and folding mechanism [36]. Following the same logic as before, we hypothezie that the in-plane rigidity provided by SP-B and SP-C in Survanta will lead to longer microbubble circulation persistence *in vivo*.

Materials and Methods

Materials

All the lipids were purchased from Avanti Polar Lipids, Inc. (Alabaster, AL), including 1,2-dipalmitoyl-sn-glycero-3-phosphocholine (DPPC), 1,2-distearoyl-sn-glycero-3-

phosphocholine (DSPC), 1,2-diarachidoyl-sn-glycero-3-phosphocholine (DAPC), 1,2-dibehenoyl-sn-glycero-3-phosphocholine (DBPC), 1,2-dilignoceroyl-sn-glycero-3-phosphocholine (DLiPC) and 1,2-distearoyl-*sn*-glycero-3-phosphoethanolamine-N-[methoxy(polyethylene glycol)-5000] (DSPE-PEG5000). Perfluorobutane gas (PFB, 99 wt % purity) was purchased from FluoroMed (Round Rock, TX). Sterile saline solution was purchased from Fisher Scientific (Pittsburg, PA). Phosphate buffered saline (PBS) (0.01 M phosphate, 0.15 M NaCl and 7.4 pH) was purchased from Sigma-Aldrich (St. Louis, MO).

Survanta was purchased from Abbott Laboratories Inc. (Abbott Park, IL), and the lipid 1, 2-dipalmitoyl-sn-glycero-3-phosphocholine (DPPC) was purchased from Avanti Polar Lipids, Inc. (Alabaster, AL). Sulfur Hexafluoride (SF_6) (98.8% purity) was purchased from Airgas Inc. (Radnor, PA) and Perfluorobutane (PFB) (99% purity) was purchased from FluoroMed, L.P. (Round Rock, TX). The female Sprague-Dawley rats, between ages of 6-8 weeks and weights of 210±20 g, were purchased from Harlan Laboratories Inc., Denver CO. Sterile saline solution for rat tail vain injections was purchased from Fisher Scientific Inc. (Pittsburg, PA). The phosphate buffered saline (PBS) (0.01 M phosphate, 0.15 M NaCl, and 7.4 pH) for microbubble preparation was purchased from Sigma-Aldrich (St. Louis, MO).

Microbubble Preparation

Lipid-coated microbubbles were prepared using a 9:1 molar ratio of lipids and lipopolymers (DSPE-PEG5000). Desired lipid mixtures were suspended in PBS solution [37]. Lipid suspension was gently mixed at 60 °C using a magnetic stirrer and hot plate for 15-20 minutes to suspend the lipids. The lipid mixture was first sonicated with a 20-kHz probe (Model 250A, Branson Ultrasonics; Danbury, CT) at low power (3 W) in order to disperse the lipid aggregates into small unilamellar vesicles (solution turned transparent) [37]. PFB gas was flowed over the surface of the lipid suspension, and higher power sonication (33 W) was used at the gas-liquid interface for 10 seconds to generate the lipid-coated microbubbles. Microbubbles were isolated from the suspension by centrifuging at 300 RCF for 3 minutes in a 30-mL syringe [37]. Concentrated microbubbles were stored, and infranatant was reused for subsequent microbubble preparation using the steps described above.

For generating pure DPPC or Survanta microbubbles, 2 mg/mL DPPC or Survanta in PBS was sonicated at low power until the suspension turned translucent. 2 mL aliquots of the lipid suspensions were placed in 3-mL glass serum vials, and the vials were capped and sealed. The vial headspace was replaced with the hydrophobic gas SF_6 or PFB using a custom gas exchange apparatus. Microbubbles were produced by shaking the vial at ~4300 Hz for 45 s using a VialMix shaker (Bristol-Myers Squibb, New York, NY) as described elsewhere [21]. Microbubbles were transferred to 3-mL syringe and washed 3 times to remove liposome and micelles by centrifuging at 300 RCF for 3 min (Model 5804, Eppendorf, Westbury, NY), as described elsewhere [38].

Isolation of 4-5 micron microbubbles was done using differential centrifugation, as described elsewhere [37]. Briefly, microbubbles above 5-μm diameter were removed by centrifuging at 70 RCF for 1 minute. The cake at the top of the syringe containing microbubbles >5 μm diameter was discarded, and the infranatant containing microbubbles <5 μm diameter was suspended in 30 mL PBS. This step was repeated 5-6 times. To remove the bubbles smaller than 4 μm diameter, the microbubble suspension was centrifuged at 100 RCF for 1 min. The infranatant containing lipid debris and bubbles >4 μm diameter was discarded, and the cake containing microbubbles >4 μm diameter was saved and suspended in 30 mL PBS. This step was repeated 4-5 times. Finally, the microbubble suspension was concentrated to 10^9 mL^{-1} and stored in the refrigerator.

Tracking Microbubble Dissolution Using Optical Microscopy

Microbubble dissolution was tracked using an optical microscope as described elsewhere. In particular, a warner instruments RC-20 perfusion chamber was modified to have two inlets and two outlets. A porous microdialysis hollow fiber (Spectra/Por Rancho Dominguez, CA) as 19kDa molecular weight cutoff was threaded through this modified chamber. This hollow fiber was used to hold the microbubbles as the solvent around the fiber and in the perfusion chamber can be exchanged without disturbing the microbubbles. Microfiber was attached to 0.2μm internal diameter tube in to which microbubbles can be injected using a 1 mL syringe. Total volume of perfusion chamber is approximately 48 μL. Initially SF_6 saturated solution was injected in to perfusion chamber. Microbubbles were added to the microfiber. Few microbubbles rose due to buoyancy and then stayed still for imaging. Syringe pump was used to inject the air-saturated solvent into the perfusion chamber at a rate of 5 mL/min. A total volume of 83 μL was added to perfusion chamber to ensure that the previous solution is purged. Microbubble will begin to show dissolution concentration gradient created after injection of air-saturated solvent. Microbubbles were imaged using an Olympus IX71 inverted microscope with a 100x air-immersion objective. CCD camera was used for time-resolved imaging of the microbubbles. ImageJ (Freeware from National institute of Health, http://rsbweb.nih.gov/ij/) was used for image processing and to measure the diameter of microbubbles.

Microbubble Stability in Diluted Suspension

Microbubbles were diluted to 10^6 mL^{-1} concentration in PBS and stirred continuously. Particle sizing was then performed using an Accusizer 280A (Particle Sizing Systems, Santa Babra, CA). The Accusizer uses the principle of laser light extinction and scattering as individual particles move through a small channel. Each measurement includes 180,000 to 200,000 counts and takes 2-3 minutes. Time-resolved measurements were done to track the change in particle number and size as a function of time. At 10^6 mL^{-1} concentration, the volume occupied by a single microbubble is ~10^6 um^3. A 5-μm diameter bubble has volume of only 65 μm^3. Therefore, each bubble had an available space of 15,000 times its volume. Considering that the Henry constant for PFB is 4.94×10^{-5} $g.m^{-3}.Pa^{-1}$ at 1-atm pressure, 10^6 μm^3 can dissolve 5×10^{-12} g of PFB. A 5-μm diameter bubble contains an order of magnitude lower amount (6.5×10^{-13} g) of PFB. Therefore, even in a closed system (i.e., no PFB can leave the solution), complete bubble dissolution will result in only 13% saturation of PFB in immediate environment.

Ultrasound Imaging

Ultrasound imaging was done to measure the *in vitro* and *in vivo* contrast persistence of microbubbles. Imaging was performed with an Acuson Sequoia 512 clinical ultrasound scanner (Siemens Healthcare USA, Malvern, PA) using a 15-MHz 15L8 linear array transducer. Measurements were done using non-linear Contrast Pulse Sequencing® (CPS) mode at 7 MHz, - 5dB gain, which resulted in a mechanical index of 0.49, as described elsewhere [39].

In Vitro Ultrasound Contrast Persistence

An agarose phantom was prepared casting 1% agarose (wt/wt) suspension in a rectangular box. A 1.7-mm outer diameter tube of was placed in the center of the gel to add a hollow channel in the agarose phantom, and it was removed after gelling was complete. The 15L8 transducer was placed over the phantom and held stationary using a custom stage to image the microbubbles. To measure the ultrasound contrast persistence *in vitro*, microbubbles were diluted to 10^6 mL^{-1} and immediately injected into the phantom. Images were acquired

in CPS mode at 5 frames/sec. Imaging was done until all visible microbubble contrast disappeared on the video monitor. Image analysis was done as described below.

In Vivo Ultrasound Contrast Persistence

All animal studies were done in accordance with the University of Colorado Boulder Institutional Animal Care and Use Committee. *In vivo* studies for microbubble circulation persistence were done in female Sprague-Dawley rats (Harlan Laboratories Inc., Denver CO) age 6-8 weeks and weight 210±20 g. The kidney was chosen for intravascular contrast because it has a high percentage of cardiac output and is close to the skin. Each rat was first anesthetized in an induction chamber using 2% isoflurane mixed in oxygen. Once sedated, the rat was placed in the prone position on a heated platform while continuously breathing 2% isoflurane. A heating pad was used to maintain body temperature of 37 °C. The heart rate was monitored using the inbuilt ECG module of the Acuson Sequoia 512. The area near the kidney was shaved with an electric clipper, hair-removal cream (Nair, Church & Dwight Co., Princeton, NJ) was used to remove any leftover hair, and blue ultrasound gel (Parkers Lab Inc., Fairfield, NJ) was used to acoustically couple the transducer to the animal. The 15L8 transducer was placed over the kidney region, guided by B-mode imaging to view the kidney, and held stationary using a custom stage.

A 27-gauge, ½-inch butterfly catheter (Terumo Medical Corporation, Somerset, NJ) was connected to a 1-mL sterile syringe, inserted into the rat tail vein and held stationary with tape. Microbubbles were diluted to 10^8 mL^{-1} in sterilized 0.9% NaCl saline solution, and a 150-μL bolus was injected while images were being recorded. The microbubble dose was 7.1×10^7 kg^{-1}, which is slightly less than the recommended dose for the FDA-approved contrast agent Definity (Lantheus Medical Imaging) of 1.2×10^8 kg^{-1}, although Definity has a considerably broader size distribution with a peak in the 1-2 μm diameter range [40]. Immediately after injection, a 100-μL bolus of saline solution was injected to flush the catheter and ensure all microbubbles were pushed into circulation. Recording was not continuous as the system was stopped for brief intervals to save and download the recorded cine loops. Images were acquired at 10 frames/sec for approximately 2-minute durations, with 0.5-1.5 min breaks in between cine loops for data processing and storage. Imaging was done until all visible microbubble contrast disappeared on the video monitor. Each rat was used for 4 measurements during a single imaging session with a waiting period of 10-20 minutes between the end of one measurement and the beginning of the next. The order of the microbubble injections was randomized for each rat. Following the imaging measurement, anesthesia was removed, and the rat was placed back into its cage.

Image Analysis

The Sequoia ultrasound scanner provided ultrasound video recordings in Diacomm format. These videos were transferred to another computer using an inbuilt DVD writer on the Sequoia system. Diacomm images were converted to JPEG using imagemagick (freeware, http://www.imagemagick.org) and were analyzed for gray scale intensity using a custom Labview program (National Instruments, Austin, TX). For *in vitro* experiments in the agarose phantom, the circular cross-section of the flow channel was used as the region of interest (ROI). For *in vivo* experiments in rats, the position of kidney was identified using B-mode images, and an ROI was drawn around the kidney and used to track the change in contrast over time. The average video intensity (AVI) was obtained by summing the CPS video intensity values for each pixel within the ROI and dividing that value by the total number of pixels within the ROI. Data was plotted and fitted to determine pharmacokinetic parameters.

A first-order pharmacokinetic model was used to model microbubble perfusion in the kidney [13, 23]. Here, the blood pool was considered as a single compartment, and uptake and elimination of contrast was assumed to be first-order [13, 23]. Thus, the contrast signal, C, was modeled as:

$$c(t) = \frac{c_0 k_1}{k_2 - k_1}\left(e^{-k_1 t} - e^{-k_2 t}\right) \quad (1)$$

where Co is the input contrast, and k_1 and k_2 are first-order rate constants describing the influx and outflux of contrast from the vasculature. Curve fitting was done in IGOR software (WaveMetrics Inc., Portland, OR) to obtain Co, k_1 and k_2.

Statistical Analysis

Each data point is the arithmetic mean of 4 independent measurements, and the corresponding error bars are one standard deviation. All statistical analyses were done in Microsoft Excel using a Students' unpaired, two-tailed t-test. Differences in pharmacokinetic properties were considered significant if the p-value was less than 0.05.

Results

Theoretical Description of Attractive Forces between Lipid Molecules

Lipid molecules self-assemble into monolayer and bilayer membranes owing to hydrophobic interactions. However, once assembled, attractive van der Waals forces dominate the inter-lipid interactions [41]. The attractive van der Waals cohesive forces are balanced by steric and hydration repulsive forces. Steric and hydration repulsive forces exist between the lipid headgroups, and steric repulsive forces exist between the acyl chains (Fig. 2A). These forces strongly depend on the lateral separation between phospholipid molecules in the monolayer plane (i.e., intermolecular distance). To a first approximation, this lateral separation is dictated by hydrophobic interactions, which drive construction and compression of the lipid monolayer. Israelachvili provided a simple relation for surfactant self-assembly, suggesting that the optimal head group area is inversely proportional to the square root of interfacial tension [42]. On the basis of this approximation, the equilibrium area per lipid in a monolayer at the gas/water interface (surface tension ~ 73 mN/m) is expected to be ~70% lower than that of a hydrated lipid bilayer (surface tension ~ 25 mN/m) [43]. Thus, since the lipid area in a gel-state PC bilayer is ~0.48 nm^2 [28, 44, 45], the inter-lipid separation in a microbubble shell is expected to be ~0.32 nm^2, which agrees with experimental findings on Langmuir monolayers at high surface pressures [46]. Lipids in monolayers are more closely packed than bilayers, and therefore the relative increase in the van der Waals interaction for each increase in carbon chain length will be more pronounced.

The attractive van der Waals energy can be calculated using a modified London equation provided by Israelachvilli [42].

$$U = \frac{3x_0^2 h\nu}{4(4\pi s_0)}\left[\frac{5}{\sigma^2} + \frac{11}{[\sigma^2 + l^2]} + \frac{11}{[\sigma^2 + 2l^2]} \ldots\right]\frac{N_0}{2} \quad (2)$$

where α is an interaction energy parameter, ε_0 is the static dielectric constant, h is Planck's constant, N_0 is Avogadro number, σ is intermolecular distance, and l is the bond length. Assuming two-dimensional hexagonal packing for lipid acyl chains, there should be 6 carbons at a distance σ from any particular carbon; and because out of these 6 carbons, 1 carbon is attached to the other acyl chain in the same lipid molecule, we can assume that 5 carbons at distance "σ" will contribute to inter-lipid attractive van der Waals interaction.

Based on these assumptions, we estimate that each additional methylene group in the lipid acyl chains increases the van der Waals attractive energy by 6.7 kJ/mol. The corresponding cohesive energy of the diacyl physopholipids in the monolayer is expected to be ~500 mJ/m^2 for 16-carbon chains, which exceeds the surface tension of water (73 mJ/m^2) and indicates that van der Waals attraction dominates the behavior of the intact microbubble shell. Increasing the carbon chain length from 16 to 24 carbons is expected to increase the cohesive energy by 50%. This will significantly enhance the microbubble stability because the rates of thermally activated phenomena, such as gas permeation through the monolayer and buckling instabilities leading to monolayer collapse, increase exponentially with the cohesive energy. Note that the van der Waals attraction falls rapidly as the lipid intermolecular distance increases (Fig. 2B). Therefore, this cohesiveness is lost as the microbubble shell dilates, and recent experiments indicate that rapidly expanding microbubbles have a surface tension near that for a clean air/water interface [4, 47]. However, our monolayer cohesion energy estimation should be valid for a dissolving microbubble, in which the shell is in a continual state of compression.

Effect of Lipid Acyl Chain Length

To measure the effect of increasing lipid acyl chain length on microbubble resistance to passive dissolution, size isolated 4-5 μm diameter lipid-coated microbubbles were diluted to 10^6 mL^{-1} concentration, and particle size and concentration were determined as a function of time. The measurement did not involve any ultrasound; microbubble stability primarily depended on the gas permeability and collapse resistance of the lipid shell. Figure 3 shows a comparison of the population distribution dynamics for microbubbles coated with the following lipids of different acyl chain lengths: DPPC (C16), DSPC (C18), DAPC (C20), DBPC (C22) and DLiPC (C24). At t=0, the population distribution for all five formulations was similar, with a peak at 5-μm diameter. As time progressed, the median diameter decreased and then stabilized at 2 μm, which is consistent with previous measurements of single microbubbles [4]. The microbubble concentration also decreased with time (Fig. 3D). The concentration-time curves did not fit a simple mono-exponential decay owing to the simultaneous changes in size and number. However, general trends can be observed with respect to lipid acyl chain length and microbubble stability. As hypothesized, the stability increased with acyl chain length from DPPC to DBPC, but there was an unexpected drop in stability for DLiPC.

To measure ultrasound contrast persistence *in vitro*, microbubbles were diluted to 10^6 mL^{-1} concentration and immediately injected into the agarose phantom, which was imaged with contrast-mode ultrasound. Figure 4A shows that there was initially no contrast when the flow channel was filled with only PBS, and that the cross-section of the flow channel became bright when microbubbles were injected. Figure 4B compares typical time-intensity curves (TICs) for microbubbles coated with each of the 5 lipids. Interestingly, the application of ultrasound accelerated the dissolution process. Previous research has shown that ultrasound can induce partial dissolution with each cycle [48, 49], likely through a physical instability in the microbubble shell [50].

The TICs were fit with the pharmacokinetic model shown in Equation 1. Results are tabulated in the supplemental information. The contrast intensity dose (C_o) increased slightly from DPPC to DSPC ($p<0.05$), but remained constant for DSPC through DLiPC. The contrast influx rate (k_1) depends on the injection speed and, as expected, was found to be independent of the coating lipid. The contrast efflux rate (k_2) is a measure of microbubble elimination and was found to decrease, corresponding to an increase in persistence, from DPPC to DSPC ($p<0.05$). The corresponding microbubble *in vitro* half-life increased monotonically from DPPC to DSPC (Fig. 4C). This result is consistent with the passive dissolution result described above. However, there was no significant change in persistence

when acyl chain length was increased from DSPC to DBPC ($p>0.05$). Again, we observed a decrease in microbubble stability from DBPC to DLiPC ($p<0.05$). This result suggests that increasing acyl chain length does not have precisely the same effect on the rate of ultrasound-mediated dissolution as it does on passive dissolution.

Finally, we measured the effect of lipid acyl chain length on *in vivo* circulation persistence. Bolus injections of 150 μL at 10^8 mL^{-1} were given while the rat kidney was imaged using contrast-enhanced ultrasound. Background intensity (prior to the injection of microbubbles) was very low, as shown in Figure 5A, but the video intensity increased significantly upon microbubble injection. The initial contrast intensities for DPPC and DLiPC microbubbles were considerably lower than for the other microbubble compositions. Figure 5B shows the TIC for the ROI encompassing the kidney. Overall, microbubble persistence decreased *in vivo* compared to *in vitro*, suggesting the roles of immune system and cardiopulmonary circulation in limiting the microbubble lifetime.

Again, the TICs were fitted with the first-order pharmacokinetic model, Equation 1. Results are tabulated in the supplemental information. Input intensity (C_o) increased from DPPC to DSPC ($p<0.05$) and then remained the same for DSPC to DBPC, followed by a decrease in intensity from DBPC to DLiPC. More importantly, we observed an increase in contrast persistence with increasing in acyl chain length. The *in vivo* half-life of DBPC was 5.08 ± 0.80 min, which was ~20-fold greater than that of DPPC, which is similar in composition to Definity® [51], and ~5-fold greater than that of DSPC, which is commonly used contrast enhanced ultrasound research [14, 52, 53]. Again, the exception to the trend was DLiPC, which showed a much lower persistence as compared to DBPC, similar to *in vitro* results. Overall, persistence of microbubbles *in vivo* was much less than that *in vitro*, suggesting the roles of circulation and the immune system in limiting contrast agent lifetime.

Effect of Lung Surfactant Proteins

We first compared the dissolution of SF_6 microbubbles coated with pure DPPC to Survanta (DPPC with SP-B and SP-C and other more fluid lipids). Microbubbles were kept in SF_6-saturated PBS and then suddenly exposed to an air-saturated environment at t=0 [4, 54]. Figure 6 shows micrographs and the change in diameter of the Survanta and pure-DPPC microbubbles over time. The initial diameter of both pure-DPPC and Survanta microbubbles was approximately same. The pure-DPPC microbubble dissolved very quickly (~0.6 min). In contrast, the Survanta microbubble dissolved in approximately 16 min. The bar charts plotted along with the dissolution curves show the rate of change in microbubble surface area with time. For pure-DPPC microbubbles, the rate of dissolution monotonically increased as microbubble size decreased. This observation is typical for Laplace-pressure driven dissolution, because the internal pressure increases with decreasing microbubble size, thus accelerating microbubble dissolution. For Survanta microbubbles, however, the dissolution rate was independent of the microbubble diameter and was discontinuous. Survanta microbubbles intermittently wrinkled and "snapped" to smaller diameters during the dissolution process, and this process is represented by spikes in the corresponding differential area bar plot. Unlike pure-DPPC, Survanta microbubbles acquired non-spherical, wrinkled shapes between the snapping events before suddenly changing geometry to a spherical shape of smaller size. Previous research has shown that this snapping process is a consequence of monolayer collapse, by which the microbubble sheds excess lipid and releases compressive stress built up in the microbubble shell owing to gas dissolution [22, 55].

We next measured the *in vitro* ultrasound contrast persistence of pure-DPPC and Survanta microbubbles by injecting them into a flow channel (Fig. 7). Survanta microbubbles were more stable, with an *in vitro* half-life of 0.96 ± 0.18 min as compared to 0.25 ± 0.09 min for

pure DPPC. The contrast dose, C_o, was higher for Survanta than for pure DPPC. The initial size and concentration of DPPC and Survanta microbubbles used for this study were the same, so the low contrast dose suggests that the dilution and injection steps may have destroyed some of the pure-DPPC microbubbles.

Finally, we measured the *in vivo* circulation persistence of microbubbles in the rat kidney (Fig. 7). As above, microbubble persistence decreased *in vivo* compared to *in vitro*. Survanta microbubbles showed a much higher contrast dose than pure-DPPC microbubbles. Additionally, the contrast persistence was higher for Survanta (half-life = 0.25 ± 0.06 min) compared to pure DPPC (0.014 ± 0.001 min).

Discussion

We hypothesized that increasing the in-plane rigidity of the lipid monolayer shell would increase the microbubble *in vivo* circulation lifetime. This hypothesis was validated for lipids DPPC (16:0) to DBPC (22:0), thus validating the rational design paradigm discussed above. However, we found that increasing increase acyl chain length had different effects on passive dissolution, *in vitro* ultrasound contrast persistence and *in vivo* circulation persistence. For passive dissolution, we measured that microbubble stability increased consistently from DPPC to DBPC, but decreased for DLiPC. This trend was also found for *in vitro* and *in vivo* experiments, and we may conclude that the passive dissolution experiment provides some predictive information on the influence of microbubble shell composition on *in vivo* circulation. This suggests that, for a given microbubble size, concentration and surface architecture (fully formed PEG5000 brush), the *in vivo* circulation persistence is largely dictated by dissolution.

The sharp rise in stability between DPPC and DSPC for all three measurement methods may be explained by a step increase in shell rigidity, which we termed the “wrinkling threshold” above owing to the observation of non-spherical shapes and surface wrinkles on individual microbubbles during dissolution. In previous studies, microbubbles coated with DSPC were found to be much more rigid than those coated with DPPC, despite the difference of only two methylene groups per acyl chain. This was observed in single-microbubble dissolution studies, where microbubbles coated with DSPC and longer chain lipids exhibited wrinkling as they dissolved, while those coated with DPPC remained smooth [22]. DSPC also was found to resist surface shear [56] and oxygen gas permeation [31], while DPPC offered no measurable resistance to these transport processes. Thus, the wrinkling transition may be a hallmark of the onset of microbubble gas permeation resistance and surface viscosity.

More evidence for the influence of the wrinkling transition on microbubble stability *in vivo* was found when comparing pure-DPPC microbubbles to Survanta. Owing to the presence of surfactant proteins SP-B and SP-C, Survanta monolayers experience in-plane rigidity, which shifts the collapse mechanism from in-plane shearing to folding and allows the monolayer to maintain compressive stress [36]. This in-plane rigidity was observed in dissolving Survanta microbubbles as wrinkling. Pure-DPPC monolayers collapse by fracture and do not hold compressive stress well, and this was observed here as continuous spherical microbubble dissolution. Thus, the results comparing Survanta microbubbles to pure-DPPC microbubbles support our conclusion that wrinkling is associated with higher *in vitro* and *in vivo* stability.

The drop in stability between DBPC and DLiPC was unexpected and forced us to reconsider our assumption that the surface microstructure was equivalent for each lipid formulation containing DSPE-PEG5000. The acyl chain length of DLiPC (C24) is six methylene groups longer than the acyl chains of DSPE-PEG5000, which may have resulted in hydrophobic mismatch [57]. This hydrophobic (height) mismatch may have facilitated microbubble

dissolution through a lower energy barrier for nucleation of collapse folds. This indicates an upper limit on the acyl chain length for the main lipid with respect to the lipopolymer emulsifier.

Conclusion

In this study, we found that relatively small changes in lipid acyl chain length resulted in a significantly prolonged circulation lifetime *in vivo*. By correlating microbubble composition and biomedical performance, we have extended the biomaterials paradigm toward the rational design of long-circulating microbubbles. The resulting design rules are: (1) in-plane monolayer rigidity leading to microbubble wrinkling is a key step towards prolonged *in vivo* circulation persistence and (2) microbubble stability is increased by using longer lipid acyl chains, with the caveat that the difference in acyl chains between the species in the shell cannot exceed 4 carbons to avoid hydrophobic mismatch. The *in vivo* half-life of the longest circulating lipid shell, DBPC was ~20-fold greater than current echocardiography contrast agents and ~5-fold greater than current research formulations. Longer circulation may be advantageous for many biomedical applications, such as ultrasound molecular imaging and ultrasound image-guided drug delivery.

Supplementary Material

Refer to Web version on PubMed Central for supplementary material.

Acknowledgments

We thank Dr. Shashank Sirsi for help with *in vivo* imaging and Dr. James Kwan for help with the gas-exchange apparatus. Funding for this work was provided by NIH R01 EB009066 and NSF CBET 1059726.

REFERENCES

[1]. Lindner JR. Microbubbles in medical imaging: current applications and future directions. Nat Rev Drug Discov. 2004; 3:527–32. [PubMed: 15173842]

[2]. Klibanov AL, Hughes MS, Wojdyla JK, Wible JH, Brandenburger GH. Destruction of contrast agent microbubbles in the ultrasound field: the fate of the microbubble shell and the importance of the bubble gas content. Acad Radiol. 2002; 9:S41–S5. [PubMed: 12019891]

[3]. Unger EC, Porter T, Culp W, Labell R, Matsunaga T, Zutshi R. Therapeutic applications of lipid-coated microbubbles. Adv Drug Deliv Rev. 2004; 56:1291–314. [PubMed: 15109770]

[4]. Kwan JJ, Borden MA. Lipid monolayer dilatational mechanics during microbubble gas exchange. Soft Matter. 2012; 8:4756–66.

[5]. Stride E. Physical principles of microbubbles for ultrasound imaging and therapy. Cerebrovasc Dis. 2009; 27(Suppl 2):1–13. [PubMed: 19372656]

[6]. Stride EP, Coussios CC. Cavitation and contrast: the use of bubbles in ultrasound imaging and therapy. Proc Inst Mech Eng H. 2010; 224:171–91. [PubMed: 20349814]

[7]. Azmin M, Harfield C, Ahmad Z, Edirisinghe M, Stride E. How do microbubbles and ultrasound interact? basic physical, dynamic and engineering principles. Curr Pharm Des. 2012; 18:2118–34. [PubMed: 22352768]

[8]. Platts DG, Fraser JF. Contrast echocardiography in critical care: echoes of the future? a review of the role of microsphere contrast echocardiography. Crit Care Resusc. 2011; 13:44–55. [PubMed: 21355829]

[9]. Tartis MS, Kruse DE, Zheng H, Zhang H, Kheirolomoom A, Marik J, et al. Dynamic microPET imaging of ultrasound contrast agents and lipid delivery. J Control Release. 2008; 131:160–6. [PubMed: 18718854]

[10]. Willmann JK, Cheng Z, Davis C, Lutz AM, Schipper ML, Nielsen CH, et al. Targeted microbubbles for imaging tumor angiogenesis: assessment of whole-body biodistribution with dynamic micro-PET in mice. Radiology. 2008; 249:212–9. [PubMed: 18695212]

[11]. Fisher NG, Christiansen JP, Klibanov A, Taylor RP, Kaul S, Lindner JR. Influence of microbubble surface charge on capillary transit and myocardial contrast enhancement. J Am Coll Cardiol. 2002; 40:811–9. [PubMed: 12204515]

[12]. Chen CC, Borden MA. The role of poly(ethylene glycol) brush architecture in complement activation on targeted microbubble surfaces. Biomaterials. 2011; 32:6579–87. [PubMed: 21683439]

[13]. Chen CC, Sirsi SR, Homma S, Borden MA. Effect of surface architecture on in vivo ultrasound contrast persistence of targeted size-selected microbubbles. Ultrasound Med Biol. 2012; 38:492–503. [PubMed: 22305060]

[14]. Chen CC, Borden MA. The role of poly(ethylene glycol) brush architecture in complement activation on targeted microbubble surfaces. Biomaterials. 2011; 32:6579–87. [PubMed: 21683439]

[15]. Chen CC, Sirsi SR, Homma S, Borden MA. Effect of surface architecture on in vivo ultrasound contrast persistence of targeted size-selected microbubbles. Ultrasound Med Biol. 2012; 38:492–503. [PubMed: 22305060]

[16]. Borden MA, Sarantos MR, Stieger SM, Simon SI, Ferrara KW, Dayton PA. Ultrasound radiation force modulates ligand availability on targeted contrast agents. Mol Imaging. 2006; 5:139–47. [PubMed: 16954028]

[17]. Borden MA, Zhang H, Gillies RJ, Dayton PA, Ferrara KW. A stimulus-responsive contrast agent for ultrasound molecular imaging. Biomaterials. 2008; 29:597–606. [PubMed: 17977595]

[18]. Toft KG, Hustvedt SO, Hals PA, Oulie I, Uran S, Landmark K, et al. Disposition of perfluorobutane in rats after intravenous injection of Sonazoid. Ultrasound Med Biol. 2006; 32:107–14. [PubMed: 16364802]

[19]. Mattrey RF. The potential role of perfluorochemicals (PFCs) in diagnostic imaging. Artif Cells Blood Substit Immobil Biotechnol. 1994; 22:295–313. [PubMed: 8087248]

[20]. Schneider M, Arditi M, Barrau M-B, Brochot J, Broillet A, Ventrone R, et al. BR1: a new ultrasonographic contrast agent based on sulfur hexafluoride-filled microbubbles. Invest Radiol. 1995; 30:451–7. [PubMed: 8557510]

[21]. Fritz TA, Unger EC, Sutherland G, Sahn D. Phase I clinical trials of MRX-115: a new ultrasound contrast agent. Invest Radiol. 1997; 32:735–40. [PubMed: 9406013]

[22]. Borden MA, Longo ML. Dissolution behavior of lipid monolayer-coated, air-filled microbubbles: effect of lipid hydrophobic chain length. Langmuir. 2002; 18:9225–33.

[23]. Sirsi S, Feshitan J, Kwan J, Homma S, Borden M. Effect of microbubble size on fundamental mode high frequency ultrasound imaging in mice. Ultrasound Med Biol. 2010; 36:935–48. [PubMed: 20447755]

[24]. Borden MA, Kruse D, Caskey C, Zhao S, Dayton P, Ferrara K. Influence of lipid shell physicochemical properties on ultrasound-induced microbubble destruction. IEEE Trans Ultrason Ferroelectr Freq Control. 2005; 52:1992–2002. [PubMed: 16422411]

[25]. Rawicz W, Olbrich KC, McIntosh T, Needham D, Evans E. Effect of chain length and unsaturation on elasticity of lipid bilayers. Biophys J. 2000; 79:328–39. [PubMed: 10866959]

[26]. Bagatolli LA, Gratton E. A correlation between lipid domain shape and binary phospholipid mixture composition in free standing bilayers: A two-photon fluorescence microscopy study. Biophys J. 2000; 79:434–47. [PubMed: 10866969]

[27]. Ipsen JH, Jørgensen K, Mouritsen OG. Density fluctuations in saturated phospholipid bilayers increase as the acyl-chain length decreases. Biophys J. 1990; 58:1099–107. [PubMed: 2291936]

[28]. Lewis BA, Engelman DM. Lipid bilayer thickness varies linearly with acyl chain length in fluid phosphatidylcholine vesicles. J Mol Biol. 1983; 166:211–7. [PubMed: 6854644]

[29]. Kim K, Choi SQ, Zasadzinski JA, Squires TM. Interfacial microrheology of DPPC monolayers at the air-water interface. Soft Matter. 2011; 7:7782–9.

[30]. Kim DH, Costello MJ, Duncan PB, Needham D. Mechanical properties and microstructure of polycrystalline phospholipid monolayer shells: novel solid microparticles. Langmuir. 2003; 19:8455–66.

[31]. Borden MA, Longo ML. Oxygen permeability of fully condensed lipid monolayers. J Phys Chem B. 2004; 108:6009–16.

[32]. Pu G, Longo ML, Borden MA. Effect of microstructure on molecular oxygen permeation through condensed phospholipid monolayers. J Am Chem Soc. 2005; 127:6524–5. [PubMed: 15869260]

[33]. Pérez-Gil J. Structure of pulmonary surfactant membranes and films: the role of proteins and lipid–protein interactions. Biochim Biophys Acta. 2008; 1778:1676–95. [PubMed: 18515069]

[34]. Holten-Andersen N, Henderson JM, Walther FJ, Waring AJ, Ruchala P, Notter RH, et al. KL4 Peptide induces reversible collapse structures on multiple length scales in model lung surfactant. Biophys J. 2011; 101:2957–65. [PubMed: 22208194]

[35]. Discher BM, Maloney KM, Schief WR, Grainger DW, Vogel V, Hall SB. Lateral phase separation in interfacial films of pulmonary surfactant. Biophys J. 1996; 71:2583–90. [PubMed: 8913596]

[36]. Pocivavsek L, Frey SL, Krishan K, Gavrilov K, Ruchala P, Waring AJ, et al. Lateral stress relaxation and collapse in lipid monolayers. Soft Matter. 2008; 4:2019–29. [PubMed: 19657472]

[37]. Feshitan JA, Chen CC, Kwan JJ, Borden MA. Microbubble size isolation by differential centrifugation. J Colloid Interface Sci. 2009; 329:316–24. [PubMed: 18950786]

[38]. Choi JJ, Feshitan JA, Baseri B, Wang S, Tung Y-S, Borden MA, et al. Microbubble-size dependence of focused ultrasound-induced blood-brain barrier opening in mice in vivo. IEEE Trans Biomed Eng. 2010; 57:145–54. [PubMed: 19846365]

[39]. Streeter JE, Gessner R, Miles I, Dayton PA. Improving sensitivity in ultrasound molecular imaging by tailoring contrast agent size distribution: in vivo studies. Mol Imaging. 2010; 9:87–95. [PubMed: 20236606]

[40]. Goertz DE, de Jong N, van der Steen AFW. Attenuation and size distribution measurements of definity (TM) and manipulated definity (TM) populations. Ultrasound Med Biol. 2007; 33:1376–88. [PubMed: 17521801]

[41]. Nagle JF. Theory of the main lipid bilayer phase transition. Ann Rev Phys Chem. 1980; 31:157–96.

[42]. Israelachvili, JN. Intermolecular and surface forces. 3rd ed. Academic Press; New York: 2011.

[43]. Feshitan JA, Boss MA, Borden MA. Magnetic resonance properties of Gd(III)-bound lipid-coated microbubbles and their cavitation fragments. Langmuir. 2012; 28:15336–43. [PubMed: 23045962]

[44]. Nagle JF, Tristram-Nagle S. Structure of lipid bilayers. Biochim Biophys Acta. 2000; 1469:159–95. [PubMed: 11063882]

[45]. Petrache HI, Dodd SW, Brown MF. Area per lipid and acyl length distributions in fluid phosphatidylcholines determined by 2H NMR spectroscopy. Biophys J. 2000; 79:3172–92. [PubMed: 11106622]

[46]. Saad SMI, Policova Z, Acosta EJ, Hair ML, Neumann AW. Mixed DPPC/DPPG monolayers at very high film compression. Langmuir. 2009; 25:10907–12. [PubMed: 19507830]

[47]. Marmottant P, van der Meer S, Emmer M, Versluis M, de Jong N, Hilgenfeldt S, et al. A model for large amplitude oscillations of coated bubbles accounting for buckling and rupture. J Acoust Soc Am. 2005; 118:3499–505.

[48]. Chomas JE, Dayton P, Allen J, Morgan K, Ferrara KW. Mechanisms of contrast agent destruction. IEEE Trans Ultrason Ferroelectr Freq Control. 2001; 48:232–48. [PubMed: 11367791]

[49]. Borden MA, Kruse D, Caskey C, Zhao S, Dayton P, Ferrara K. Influence of lipid shell physicochemical properties on ultrasound-induced microbubble destruction. IEEE Trans Ultrason Ferroelectr Freq Control. 2005; 52:1992–2002. [PubMed: 16422411]

[50]. Thomas DH, Butler M, Anderson T, Emmer M, Vos H, Borden M, et al. The “quasi-stable” lipid shelled microbubble in response to consecutive ultrasound pulses. Appl Phys Lett. 2012; 101

[51]. Imaging LM. Definity package insert. 2011

[52]. Klibanov AL. Ligand-carrying gas-filled microbubbles: ultrasound contrast agents for targeted molecular imaging. Bioconjugate Chem. 2005; 16:9–17.

[53]. Gessner RC, Streeter JE, Kothadia R, Feingold S, Dayton PA. An in vivo validation of the application of acoustic radiation force to enhance the diagnostic utility of molecular imaging using 3-D ultrasound. Ultrasound Med Biol. 2012; 38:651–60. [PubMed: 22341052]

[54]. Kwan JJ, Borden MA. Microbubble dissolution in a multi-gas environment. Langmuir. 2010; 26:6542–8. [PubMed: 20067292]

[55]. Pu G, Borden MA, Longo ML. Collapse and shedding transitions in binary lipid monolayers coating microbubbles. Langmuir. 2006; 22:2993–9. [PubMed: 16548548]

[56]. Kim DH, Costello MJ, Duncan PB, Needham D. Mechanical properties and microstructure of polycrystalline phospholipid monolayer shells: Novel solid microparticles. Langmuir. 2003; 19:8455–66.

[57]. Marsh, D. Handbook of lipid bilayers. CRC; Boca Raton: 1990.

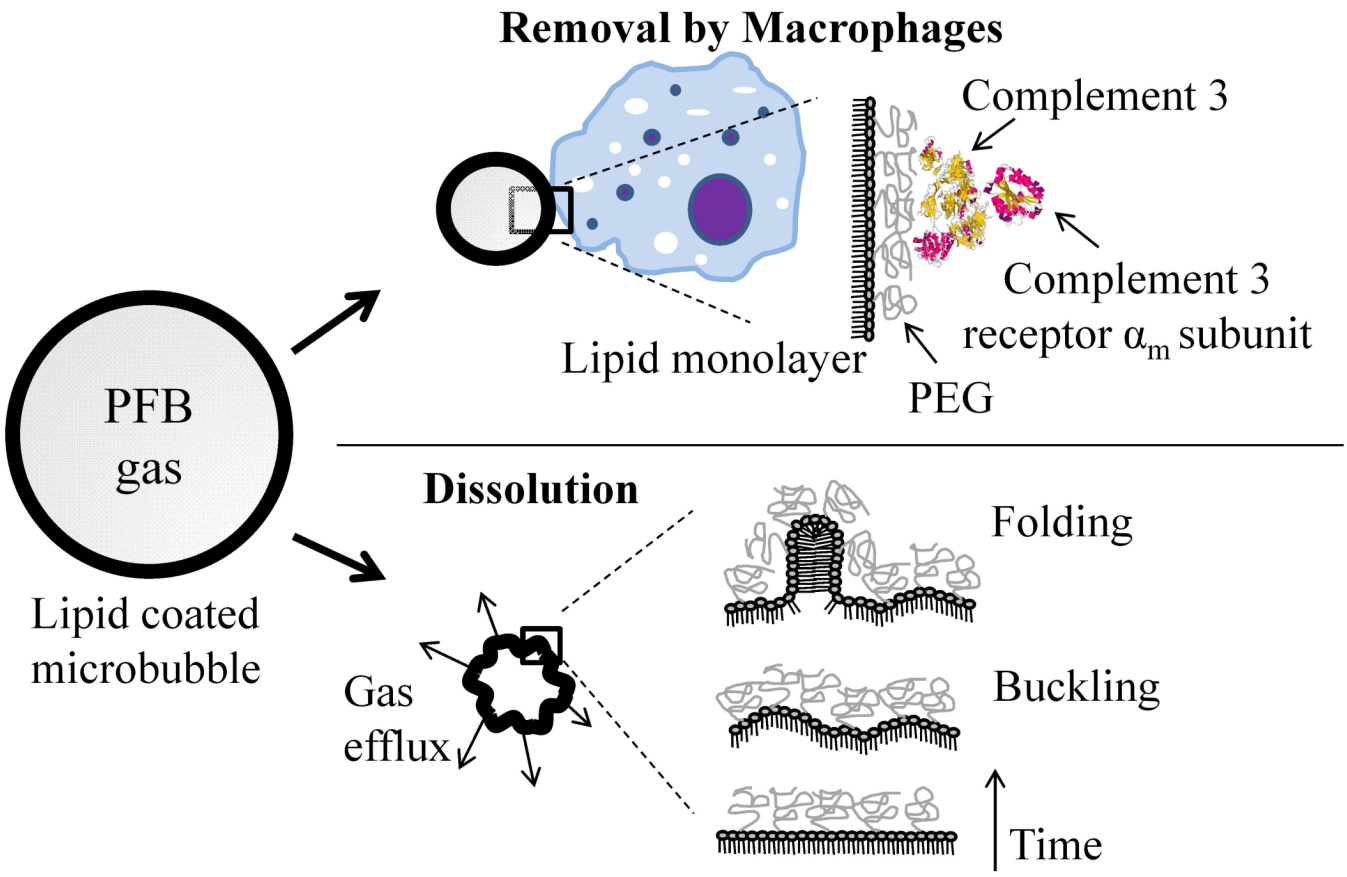

Figure 1.
Schematic representation of the two key mechanisms for removal of lipid-coated microbubbles from *in vivo* circulation. (Top) shows phagocytic removal by macrophages, which is mediated by complement C3b binding to the microbubble surface. (Bottom) shows dissolution into the bloodstream. Rigid lipid monolayers show wrinkling during dissolution owing to enhanced cohesiveness between the lipid constituents.

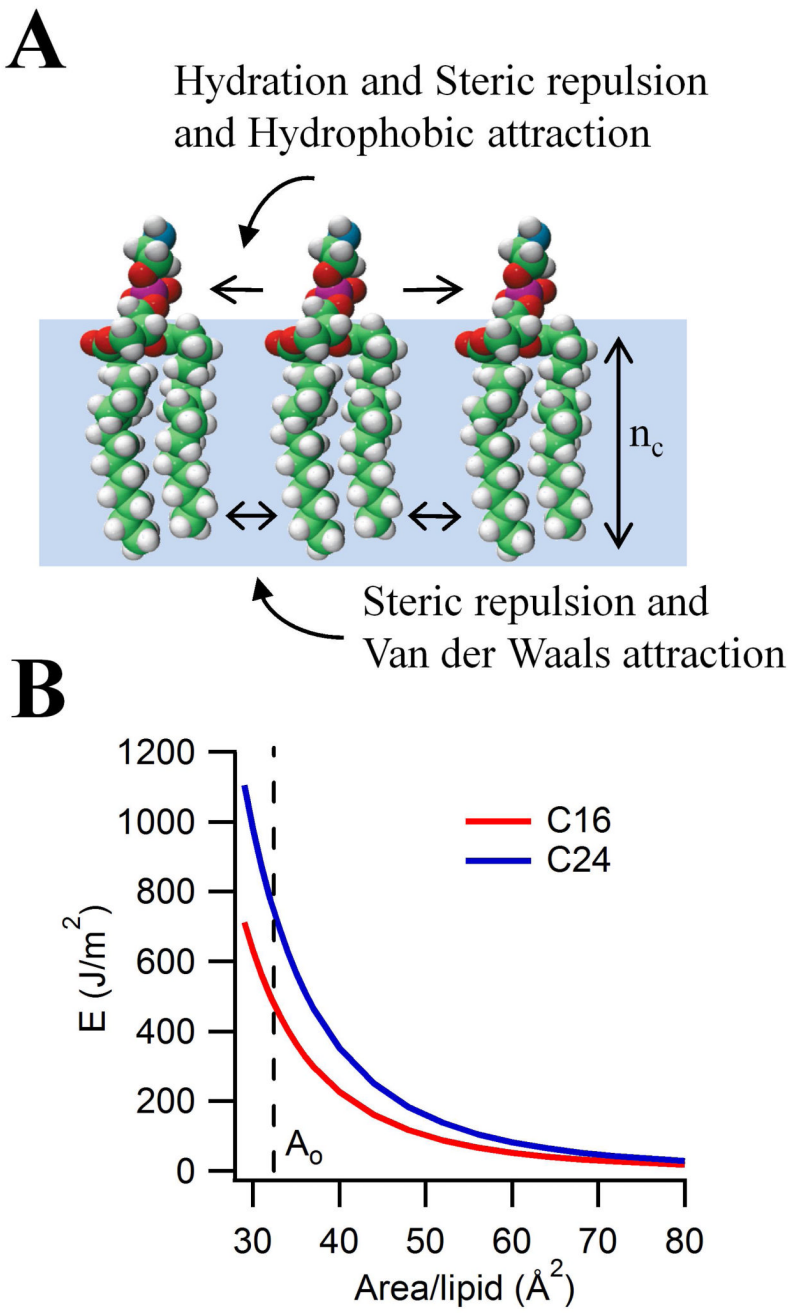

Figure 2.

Inter-lipid interactions. A) Schematic showing van der Waals and hydrophobic forces balancing hydration and steric repulsion forces. B) Attractive van der Waals forces between the lipids were calculated using the London equation, Equation 1. Also shown is the expected area per molecule for lipid-coated microbubbles (A_0). The attractive van der Waals force increases with acyl chain length. This effect is more pronounced for monolayers compared to bilayers.

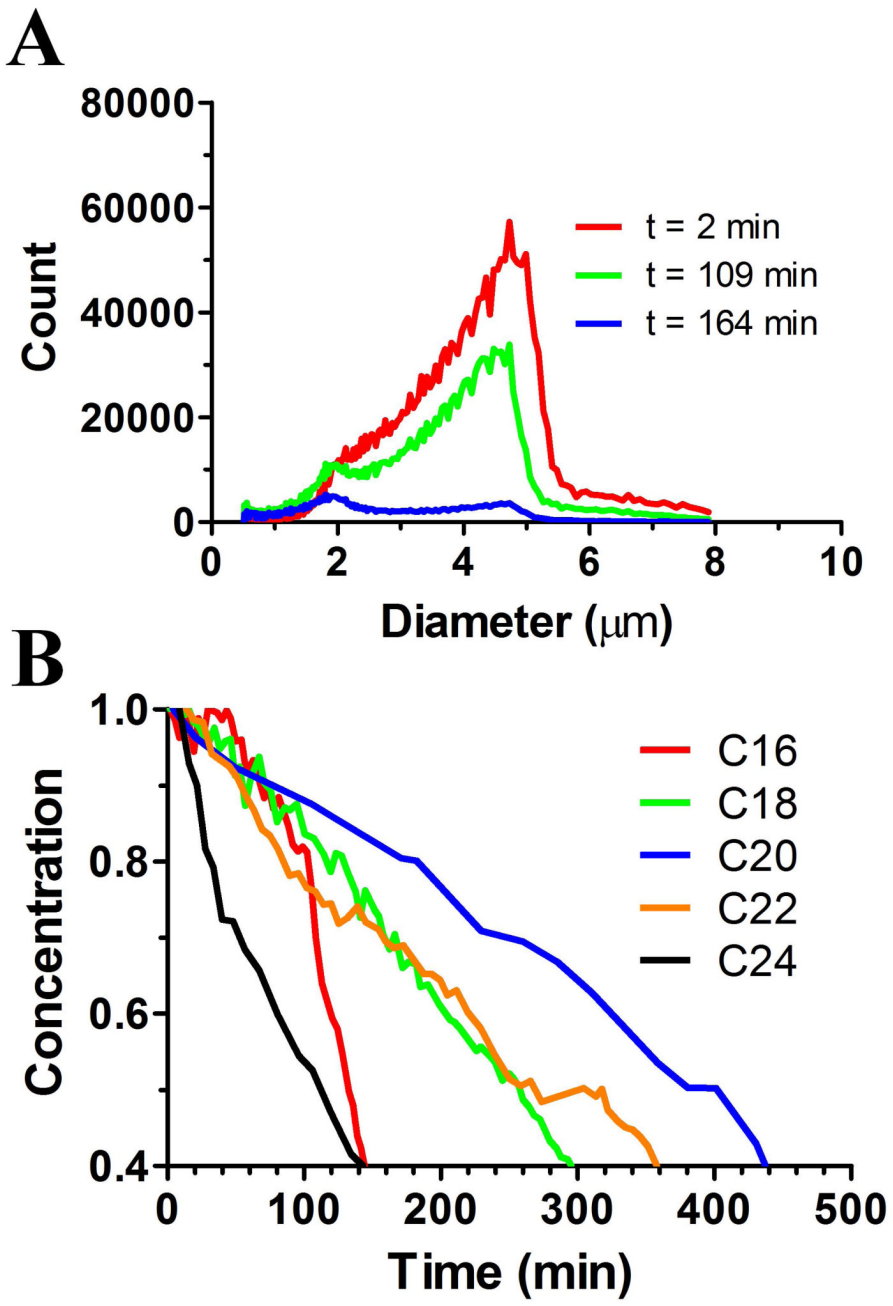

Figure 3.

Effect of lipid acyl chain length on microbubble stability to dilution. (A) Representative size distributions of microbubbles coated with DPPC. At time=0, microbubbles were diluted to the concentration of 10^6 mL^{-1} in PBS, and the size distribution was tracked as function of time using an Accusizer. (B) Representative microbubble concentration versus time curves for each lipid acyl chain length. Only microbubbles between 0 and 8 μm were counted. As hypothesized, the rate of microbubble dissolution decreased with increasing acyl chain length, but only for DPPC (C16:0) through DBPC (C22:0). Surprisingly, the dissolution rate increased significantly from DBPC to DiLiPC (C24:0).

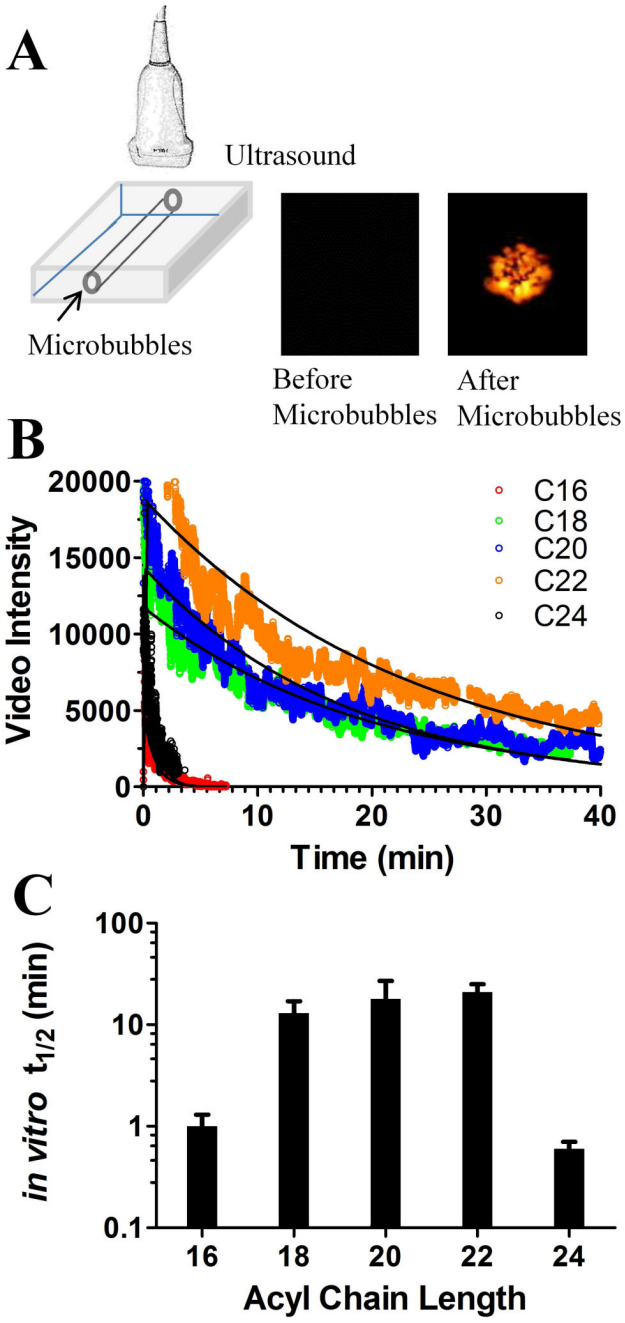

Figure 4.

Effect of lipid acyl chain length on microbubble stability to ultrasound. (A) Schematic of the agarose phantom with a flow channel used to measure the *in vitro* ultrasound contrast persistence of microbubbles. Ultrasound images are shown of the agarose phantom before and after the injection of microbubbles at concentration of 10^6 mL^{-1}. (B) Typical average video intensity as function of time for each microbubble encapsulation (n=4). (C) *In vitro* half-life $t_{1/2}$ for ultrasound contrast. Half-life was determined by fitting the pharmacokinetic model (Equation 1) to the time-intensity curves. As hypothesized, the rate of microbubble dissolution decreased with increasing acyl chain length, but only for DPPC (C16:0) through

DBPC (C22:0). Microbubbles coated with DPPC and DiLiPC were significantly less stable to ultrasound exposure than those coated with the other lipids.

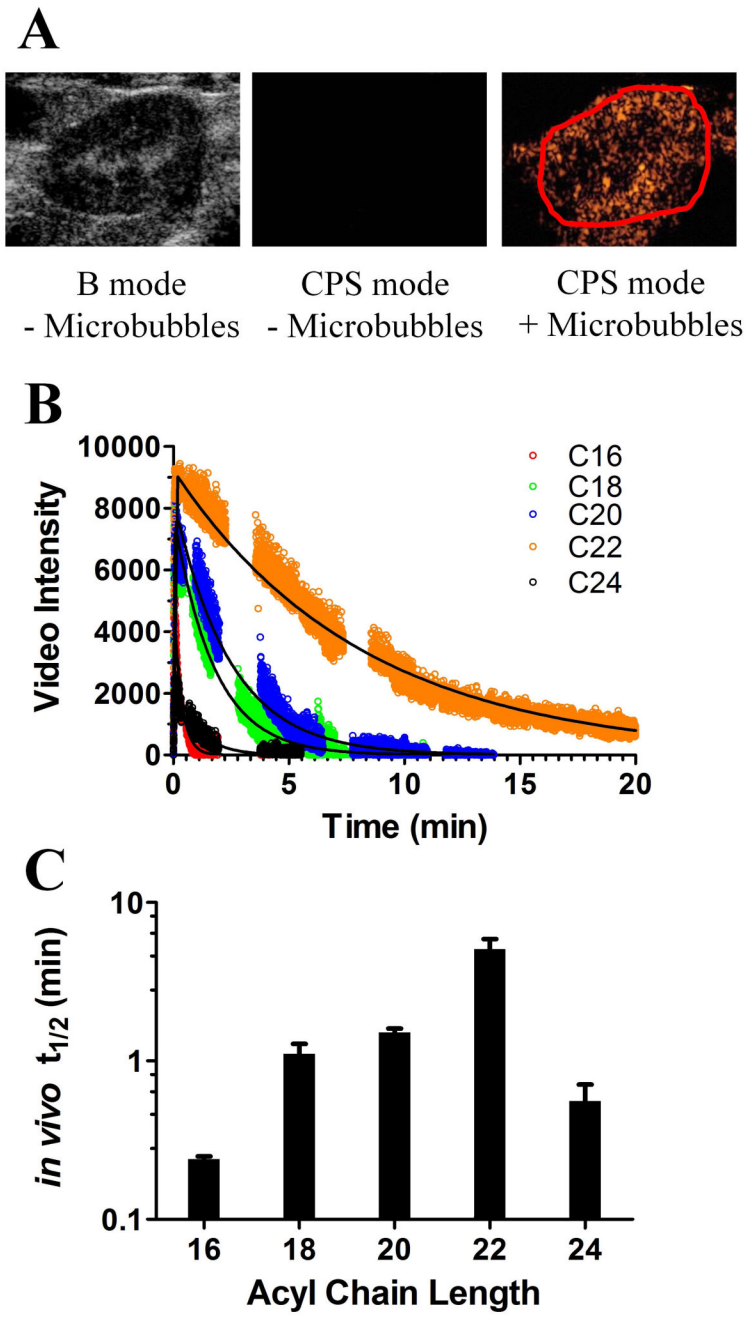

Figure 5.

Effect of lipid acyl chain length on in vivo ultrasound contrast persistence. (A) Ultrasound images of the rat kidney in B-mode and CPS mode before and after injection of microbubbles. The red line shows the region of interest (ROI) drawn around kidney (identified from B-mode imaging). (B) Time-intensity curves for ROI plotted as a function of time for each microbubble encapsulation. (C) *In vivo* half-life $t_{1/2}$ for ultrasound contrast. Half-life was determined by fitting the pharmacokinetic model (Equation 1) to the time-intensity curves. As hypothesized, the rate of microbubble dissolution decreased with increasing acyl chain length, but only for DPPC (C16:0) through DBPC (C22:0).

Microbubbles coated with DPPC and DiLiPC were significantly less stable to in vivo than those coated with the other lipids.

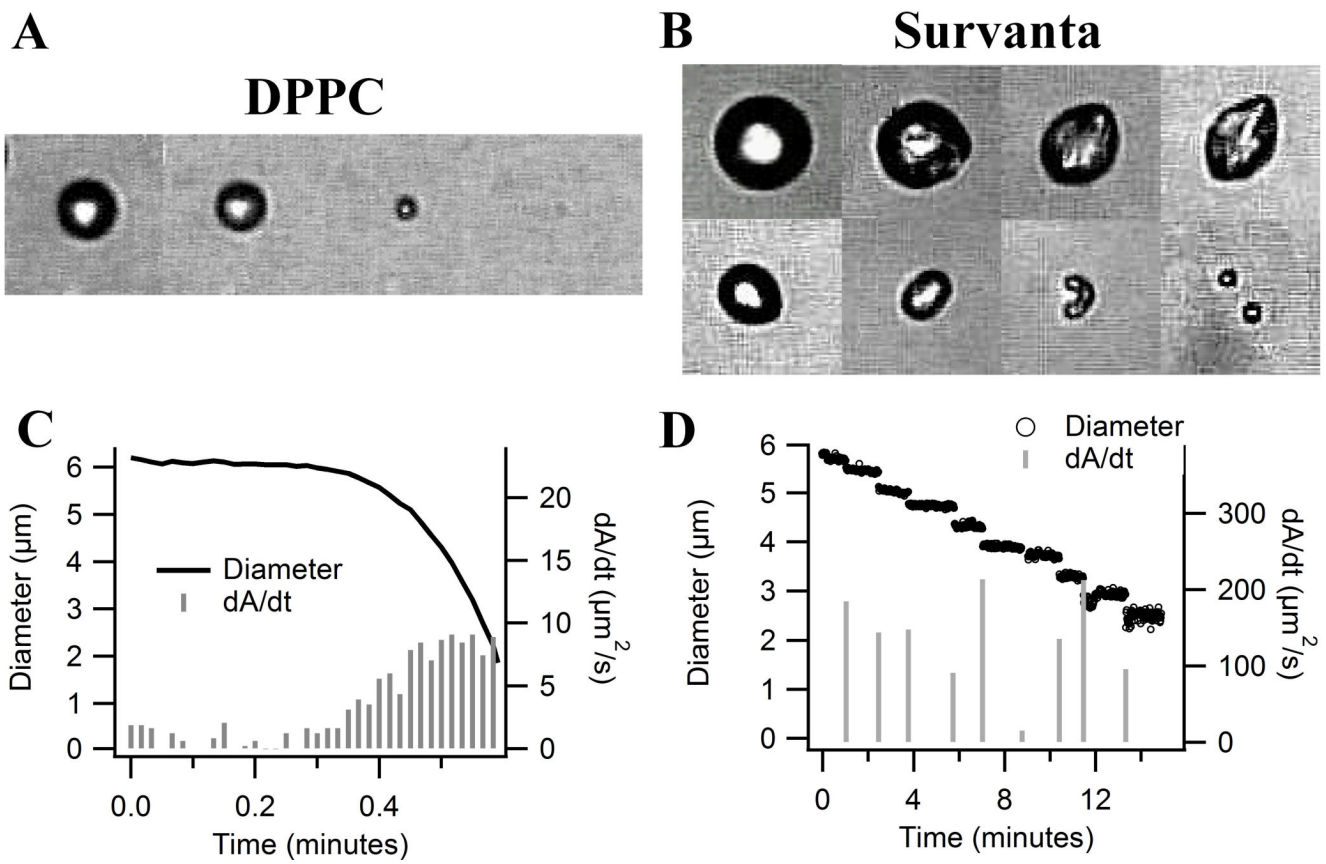

Figure 6.

Effect of surfactant proteins on microbubble dissolution. Shown are sequential bright-field microscope images for dissolution of (A) DPPC and (B) Survanta microbubbles. DPPC microbubbles remained spherical, while Survanta microbubbles attained non-spherical, wrinkled shapes during dissolution. Plots show diameter versus time for SF_6 microbubbles coated with C) DPPC and D) Survanta after exposure to an air-saturated environment. DPPC shows continuous dissolution, while Survanta shows discontinuous “wrinkling” dissolution. The plots also show the rate of change in area as bars. For DPPC, the rate of change in area increased monotonically as the microbubble shrank. For Survanta, the rate of change in area was intermittent and independent of the microbubble diameter.

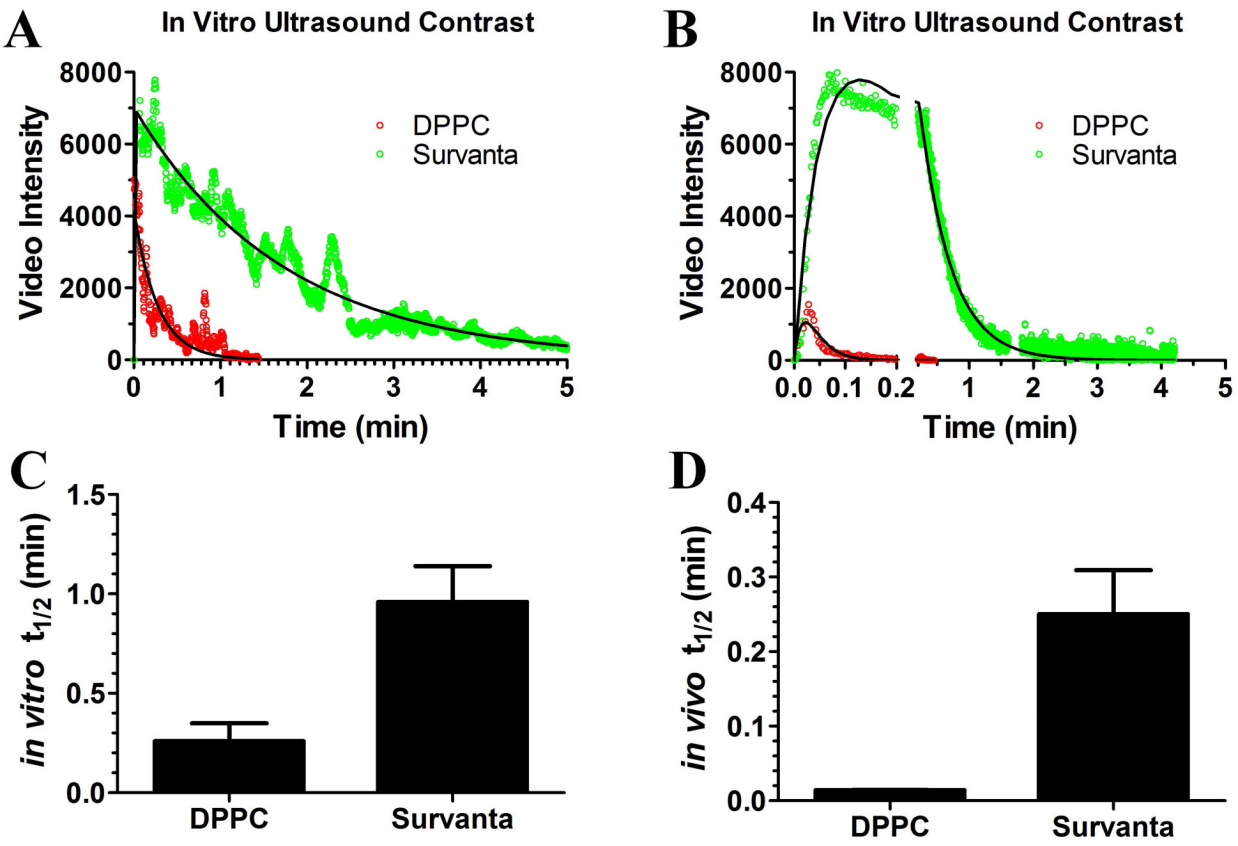

Figure 7.

Effect of surfactant proteins on ultrasound contrast persistence of microbubbles. Shown are time-intensity curves for (A) in vitro and (B) in vivo CPS imaging. The data were fit to the pharmacokinetic model in Equation 1. Using the fit, the half-life was determined (C) in vitro and (B) in vivo. In both cases, the Survanta microbubbles, which contain surfactant proteins and exhibit wrinkling during dissolution, were significantly more stable than pure DPPC microbubbles.